SUPPLEMENTARY MATERIAL

Subconductance states in NMDA receptor variants are Ca^{2+} impermeable and arise at the M2 loop

Kysilov et al

Supplementary Table 1. Phenotypical characteristics of *de novo* missense variants at GluN1 M641 and homologous positions in GluN2A (V639) and GluN2D (V667) and at the GluN1 (N616) and GluN2A (N614) N-sites.

Gene	Variant	Phenotype	Source
GRIN1	GluN1 N616S	ID	ClinVar
GRIN1	GluN1 M641I	CVI, DD, EOEE, Epi, MD, ID, cerebral atrophy, sleep disorder	(Ohba *et al.*, 2015); (Xu *et al.*, 2021); (Xu *et al.*, 2024); ClinVar
GRIN1	GluN1 M641L	DD, Epi, EOEE, MD, ID	(Pironti *et al.*, 2018); (Xu *et al.*, 2024); ClinVar
GRIN1	GluN1 M641V	CVI, DD, ID	(Xu *et al.*, 2024); ClinVar
GRIN1	GluN1 M641T	ID	ClinVar
GRIN2A	GluN2A N614S	Aphasia, ataxia, DD, Epi, ID, MD	(Farwell *et al.*, 2015); (Strehlow *et al.*, 2019); (von Stulpnagel *et al.*, 2017); ClinVar
GRIN2A	GluN2A V639I	Epi, Landau-Kleffner syndrome	(Xu *et al.*, 2024); ClinVar
GRIN2D	GluN2D V667I	CVI, Epi, EOEE, DD, MD, cerebral atrophy, sleep disorder	(Li *et al.*, 2016); (XiangWei *et al.*, 2019); ClinVar

CVI, cortical visual impairment; *DD*, developmental delay; *EOEE*, early-onset epileptic encephalopathies; *Epi*, epilepsy/seizures; *ID*, intellectual disability; *MD*, movement disorder. Variants indicated by 'ClinVar' are found in ClinVar but not gnomAD and thus classified as pathogenic (Nebet *et al.*, 2025). Note ClinVar has a limited description of clinical phenotypes.

Supplementary Table 2 (relates to Figure 3 and Supplementary Figure 1). Single channel properties of wild-type and disease-associated variants at GluN1-M641 co-expressed with GluN2A.

Construct	*i*		*Eq. Po*		*MCT*	*MOT*	
	main *pA*	**sub** *pA*	**main**	**sub**	*ms*	**main** *ms*	**sub** *ms*
N1/N2A	-7.3 ± 0.2	-4.2 ± 0.2	0.52 ± 0.03	0.021 ± 0.003	4.7 ± 0.5	4.4 ± 0.4	0.23 ± 0.03
N1(M641I)/ N2A	-6.6 ± 0.3	-2.8 ± 0.1***	0.29 ± 0.04***	0.14 ± 0.02^^^	19.8 ± 2.6^^^	3.9 ± 0.3	2.0 ± 0.2^^^
N1(M641L)/ N2A	-7.4 ± 0.6	-2.9 ± 0.3**	0.59 ± 0.06	0.023 ± 0.003	4.5 ± 0.7	3.9 ± 0.5	0.21 ± 0.03
N1(M641V)/ N2A	-7.6 ± 0.3	-3.2 ± 0.2**	0.32 ± 0.07*	0.021 ± 0.007	38.8 ± 11.5^	7.1 ± 1.5	0.39 ± 0.06^
N1(M641T)/ N2A	-7.9 ± 0.4	-3.5 ± 0.2*	0.12 ± 0.02***	0.016 ± 0.002	16.5 ± 5.3	1.5 ± 0.4***	0.14 ± 0.02*

Values shown are mean ± S.E.M. for single-channel current amplitude (*i*), equilibrium open probability (eq. P_o), mean closed time (MCT), and mean open time (MOT) either for the main or the subconductance (sub) level. Single channel currents were recorded in the on-cell mode at -100 mV at pH 7.4 and analyzed in QuB using a comparable model for all constructs (see Materials & Methods). Eq. P_o is the fractional occupancy of the open states in the entire single-channel recording, including long lived closed states. Total events (#of patches): **N1/N2A**, 3,734,783 (14); N1(M641I)/N2A, 1,465,377 (12); N1(M641L)/N2A, 1,828,785 (7); N1(M641V)/N2A, 1,004,285 (8); N1(M641T)/N2A, 2,070,403 (6).

Tagged values are significantly less *(*$p < 0.05$, **$p < 0.01$, or ***$p < 0.001$*) or greater *(^$p < 0.05$, ^^$p < 0.01$, or ^^^$p < 0.001$*) than wild type (*two-tailed Student's t-test, unpaired*).

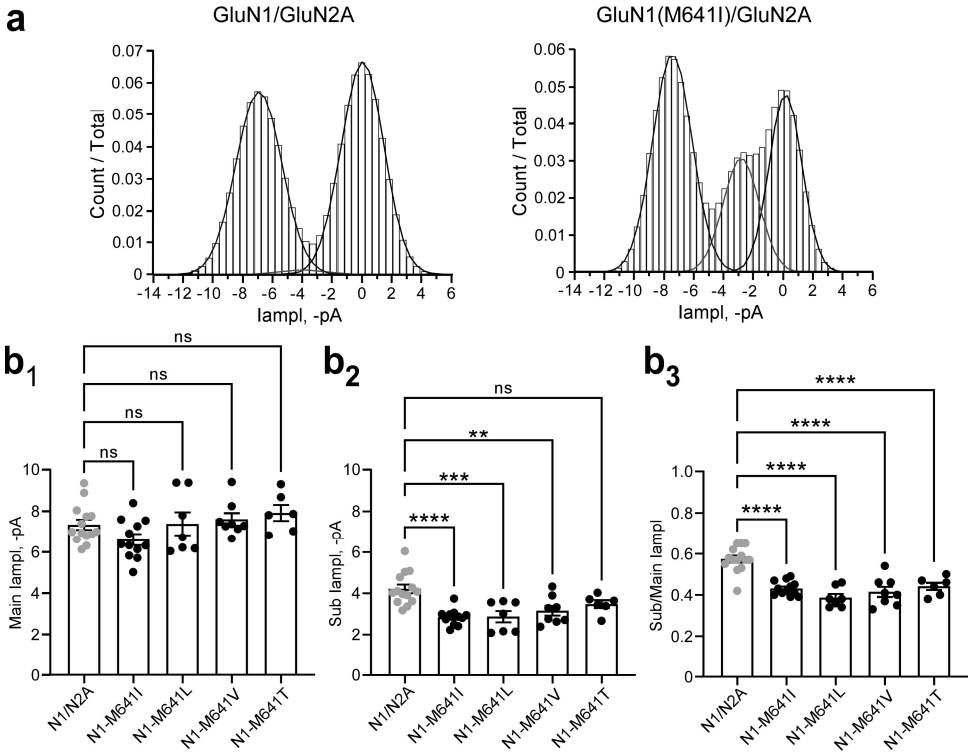

Supplementary Figure 1 (relates to Figure 3 and Supplementary Table 2). Current amplitudes for the main and subconductance levels for wild-type and disease-associated variants at GluN1-M641 co-expressed with GluN2A.

(a) All-points amplitude histograms for GluN1/GluN2A (*left*) and GluN1(M641I)/GluN2A (*right*). Fits highlight the closed and main conductance levels (black lines) or the subconductance level (red line).

(b) Bar graphs (mean ± SEM) showing current amplitudes for main (**b**$_1$) and subconductance (**b**$_2$) and the ratio between the Sub and Main (Sub/Main) conductance levels (**b**$_3$) for GluN1 M641 variants co-expressed with GluN2A.

Statistical comparisons were performed using one-way ANOVA with post hoc Dunnett tests versus wild-type (**p < 0.01, ***p < 0.005, ****p < 0.001, ns not significant).

Supplementary Table 3 (relates to Figure 4 and Supplementary Figure 2). Single channel properties of wild-type and M641 variants co-expressed with GluN2B, GluN2C, or GluN2D.

Construct	*i*		*Eq. Po*		*MCT*	*MOT*	
	main *pA*	sub *pA*	main	sub	*ms*	main *ms*	sub *ms*
N1/N2B	-6.9 ± 0.2	-3.8 ± 0.3	0.14 ± 0.02	0.009 ± 0.002	28.7 ± 2.9	4.3 ± 0.4	0.35 ± 0.12
N1(M641I)/ N2B	-6.9 ± 0.3	-3.0 ± 0.1	0.010 ± 0.003***	0.007 ± 0.003	1084± 317^	3.5 ± 1.2	1.9 ± 0.4^
N1(M641L)/ N2B	-7.1 ± 0.5	-2.9 ± 0.2	0.22 ± 0.04	0.019 ± 0.003^	30.9 ± 5.2	5.0 ± 0.6	0.61 ± 0.17
N1/N2C	-4.9 ± 0.1	-2.5 ± 0.1	0.028 ± 0.007	0.003 ± 0.001	42 ± 11	0.87 ± 0.17	0.30 ± 0.06
N1(M641I)/ N2C	-5.9± 0.3^	-2.6 ± 0.2	0.003 ± 0.0005**	0.003 ± 0.0004	315 ± 100	1.9 ± 0.4	0.58 ± 0.12
N1/N2D	-5.5 ± 0.3	-3.0 ± 0.1	0.038 ± 0.002	0.004 ± 0.001	29 ± 8	1.5 ± 0.4	0.51 ± 0.18
N1(M641I)/ N2D	-6.3 ± 0.5	-2.8 ± 0.2	0.005 ± 0.001***	0.003 ± 0.001	125 ± 61	0.69 ± 0.14	0.44 ± 0.11

Values shown are mean ± S.E.M. Single channels records analyzed and displayed as in Supplementary Table 2.

Total events (# of patches): **N1/N2B**, 183,419 (5); N1(M641I)/N2B, 26,016 (7); N1(M641L)/N2B, 275,140 (6); **N1/N2C**, 169,580 (9); N1(M641I)/N2C, 22,462 (5); **N1/N2D**, 224,755 (5); N1(M641I)/N2D, 136,104 (6).

Tagged values are significantly less (or faster) *(*$p < 0.05$, **$p < 0.01$, or ***$p < 0.001$)* or greater (or slower) *(^$p < 0.05$, ^^$p < 0.01$, or ^^^$p < 0.001$)* than wild type (*t-test*) *two-tailed Student's t-test, unpaired*).

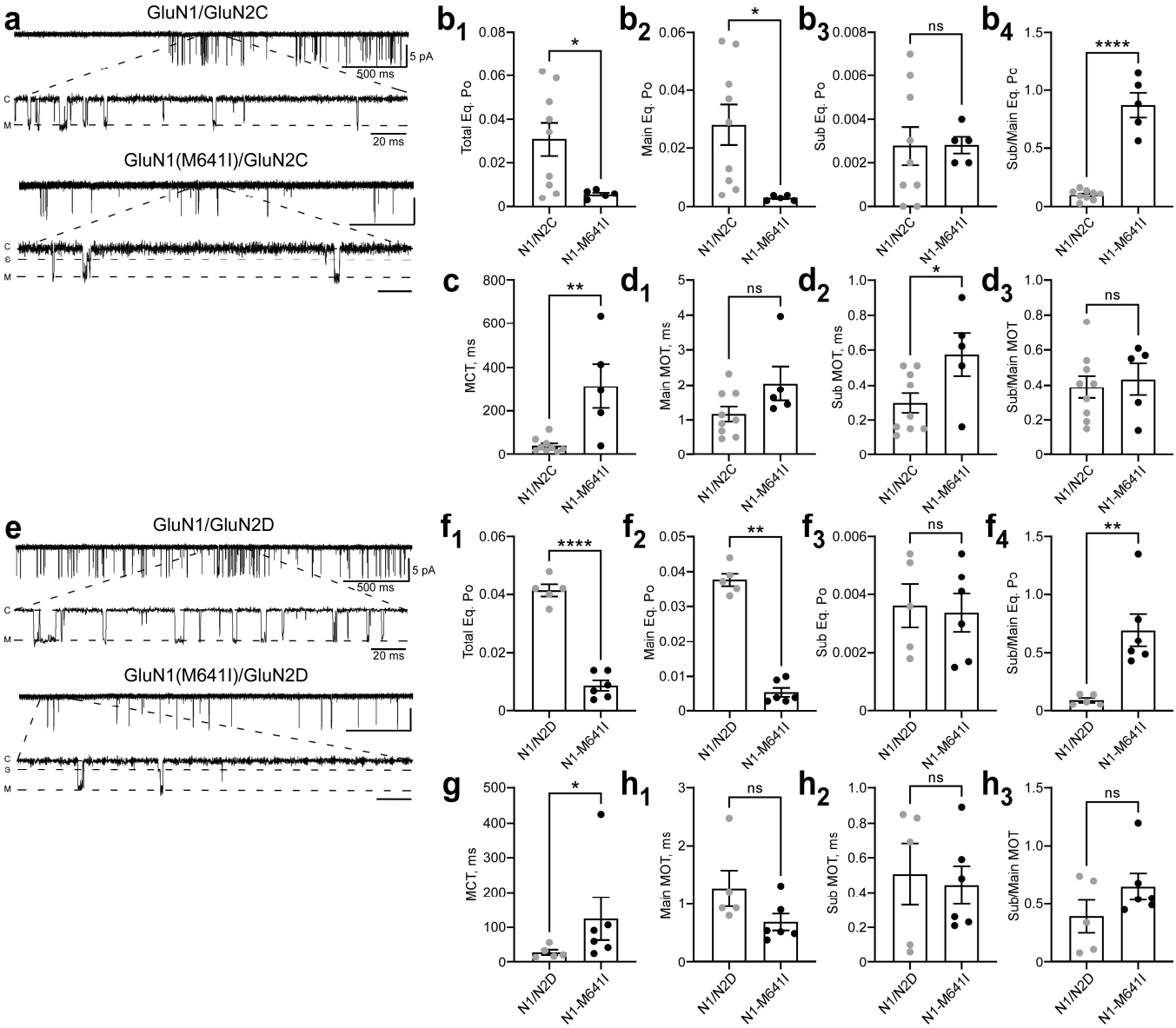

Supplementary Figure 2 (relates to Figure 4). GluN1(M641I) dramatically reduces main conductance open probability when expressed with GluN2C or GluN2D but retains a prominent subconductance state.

(**a**) Single-channel currents from human GluN1/GluN2C and GluN1(M641I)/GluN2C receptors. Data recorded and displayed as in Figure 3A, except for the filtering frequencies: the upper trace was filtered at 2 kHz, and the lower trace was filtered at 5 kHz.

(**b**) Bar graphs (mean ± SEM) showing equilibrium open probabilities for constructs in panel A.

(**c & d**) Bar graphs (mean ± SEM) showing MCT (**c**) and MOT (**d**).

(**e**) Single-channel currents from human GluN1/GluN2D and GluN1(M641I)/GluN2D receptors. Data recorded and displayed as in Figure 3A, with the filtering frequencies are as in panel A

(**f**) Bar graphs (mean ± SEM) showing equilibrium open probabilities for constructs in panel E.

(**g & h**) Bar graphs (mean ± SEM) showing MCT (**g**) and MOT (**h**).

Statistical analysis was performed by unpaired t-test (*p < 0.05, **p < 0.01, ****p < 0.001, ns not significant).

Relative to GluN1a/GluN2A, wild type GluN1a/GluN2C and GluN1a/GluN2D have strongly reduced activity but a prominent subconductance level when recorded in external Ca^{2+} (Traynelis *et al.*, 2010).

Under our conditions, specifically in the absence of external Ca^{2+}, wild-type GluN1a/GluN2C (Total Eq. Po, 0.031 ± 0.008, n = 5)(Supplementary Figure $2b_1$, Supplementary Table 3) and GluN1a/GluN2D (Total Eq. Po, 0.042 ± 0.003, n = 5)(Supplementary Figure $2f_1$, Supplementary Table 3) have extremely low levels of activity, especially relative to GluN1a/GluN2A, but lack a prominent subconductance level (Supplementary Figure $2b_3$, f_3) presumably because we recorded in the absence of Ca^{2+}. Because of their low level of activity, we used statistical approaches (Colquhoun & Hawkes, 1990; Dravid *et al.*, 2008) to verify that only a single active channel was active in these patches (Supplementary Figure 4).

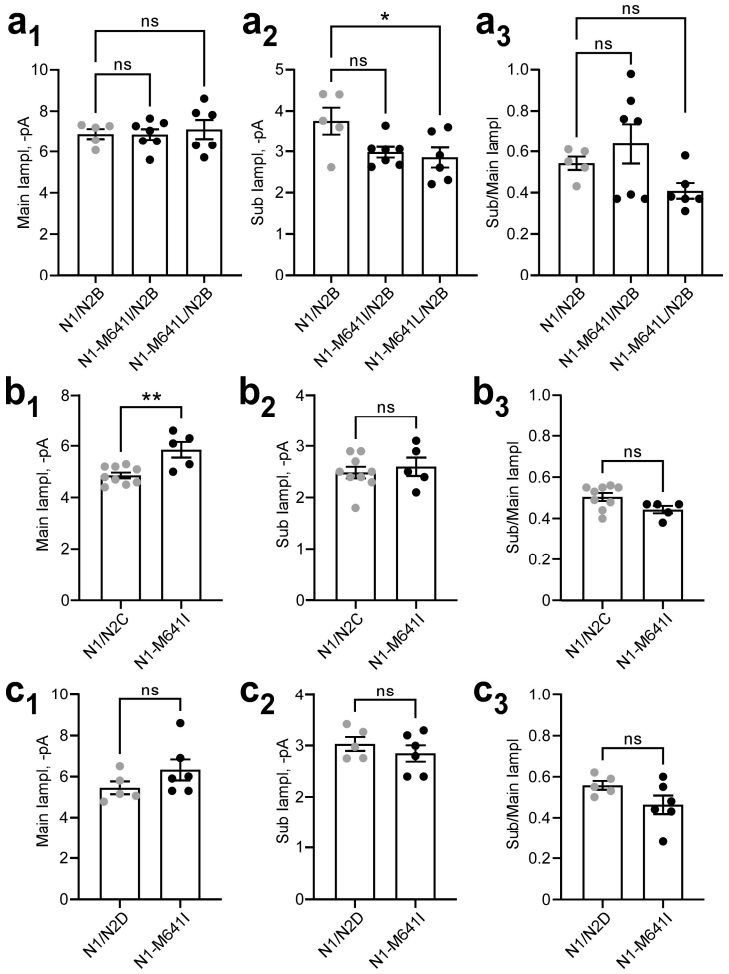

Supplementary Figure 3 (relates to Figure 4 and Supplementary Figure 2). Current amplitudes for main and subconductance levels for GluN1-M641 variants co-expressed with GluN2B, GluN2C, or GluN2D.

(**a-c**) Bar graphs (mean ± SEM) showing current amplitudes for main and subconductance levels for GluN1 M641 variants co-expressed with GluN2B (**a**), GluN2C (**b**), or GluN2D (**c**).

Statistical comparisons were performed using one-way ANOVA with post hoc Dunnett tests versus wild-type (**a**) or using an unpaired t-test (**b & c**) (*$p < 0.05$, **$p < 0.01$, ns not significant).

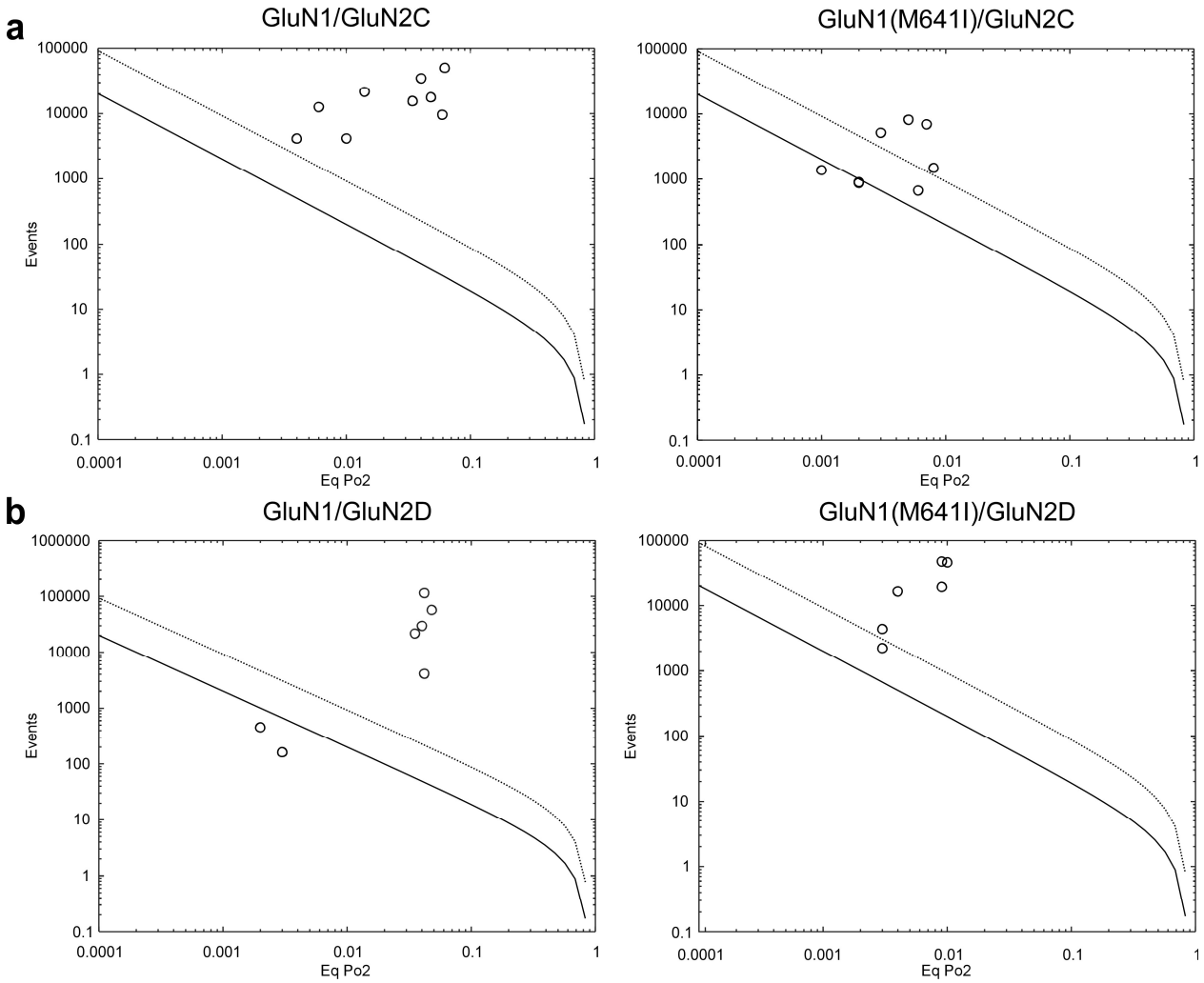

Supplementary Figure 4 (relates to Supplementary Figure 2). Statistical determination of single channel GluN2C and GluN2D patches.

(a & b) Plots used to calculate confidence that there is a single channel in the patch (Colquhoun & Hawkes, 1990; Dravid *et al.*, 2008). The black line reflects a ~50% confidence threshold while the dashed line reflects a ~99% confidence threshold. Data points are for GluN1/GluN2C and GluN1(M641I)/GluN2C (**a**) or GluN1/GluN2D and GluN1(M641I)/GluN2D (**b**). Only recordings above the 50% line were used for analysis.

Supplementary Table 4 (relates to Figure 5 and Supplementary Figure 2). Single channel properties of wild-type and GluN2A-V639I or GluN2D-V667I co-expressed with GluN1.

Construct	*i*		*Eq. Po*		*MCT*	*MOT*	
	main *pA*	**sub** *pA*	**main**	**sub**	*ms*	**main** *ms*	**sub** *ms*
N1/N2A	-7.0 ± 0.3	-4.0 ± 0.2	0.59 ± 0.03	0.021 ± 0.002	3.2 ± 0.3	4.1 ± 0.3	0.18 ± 0.04
N1/ N2A(V639I)	-6.8 ± 0.2	-3.2 ± 0.2*	0.91 ± 0.02^^^	0.031 ± 0.006	1.2 ± 0.1***	7.7 ± 0.04^	0.42 ± 0.12
N1/N2D	-5.5 ± 0.3	-3.0 ± 0.1	0.038 ± 0.002	0.004 ± 0.001	29 ± 8	1.3 ± 0.3	0.51 ± 0.18
N1/ N2D(V667I)	-4.9 ± 0.2	-2.1 ± 0.2**	0.70 ± 0.09^^^	0.012 ± 0.003^	1.9 ± 0.4*	5.9 ± 1.7	0.24 ± 0.02**

Values shown are mean ± S.E.M. Single channels records analyzed and displayed as in Supplementary Table 2.
Total events (# of patches): **N1/N2A**, 1,552,500 (7); N1/N2A(V639I), 627,423 (5); **N1/N2D**, 224,755 (5); N1/N2D(V667I), 975,063 (6).

Tagged values are significantly less (or faster) *(*p < 0.05, **p < 0.01, or ***p < 0.001*) or greater (or slower) *(^p < 0.05, ^^p < 0.01, or p < 0.001*) than wild type (*t-test*) *two-tailed Student's t-test, unpaired*).

Supplementary Table 5 (relates to Figure 7). Single channel properties of wild-type and variants (N-to-S) or mutations (N-to-A) at the GluN1 and GluN2A N-sites.

Construct	*i*		*Eq. Po*		*MCT*	*MOT*	
	main *pA*	sub *pA*	main	sub	*ms*	main *ms*	sub *ms*
N1/N2A	-7.3 ± 0.2	-4.2 ± 0.2	0.52 ± 0.03	0.021 ± 0.003	4.7 ± 0.5	4.4 ± 0.4	0.23 ± 0.03
N1(N616S)/ N2A	-8.5 ± 0.6	-3.4 ± 0.3	0.014 ± 0.003***	0.40 ± 0.09^^^	2.8 ± 0.3**	1.0 ± 0.2***	2.6 ± 1.5
N1(N616A)/ N2A	-8.5 ± 0.2^^	-3.8 ± 0.1	0.046 ± 0.013***	0.45 ± 0.07^^	4.7 ± 1.7	2.2 ± 0.4**	3.6 ± 0.9^
N1/ N2A(N614S)	-8.6 ± 0.5	-5.1 ± 0.4	0.34 ± 0.04**	0.28 ± 0.05^^	3.0 ± 0.5*	3.6 ± 0.7	3.0 ± 1.4
N1/ N2A(N614A)	-9.2 ± 0.5^	-4.0 ± 0.8	0.28 ± 0.04**	0.21 ± 0.03^^	10.0 ± 2.9	2.7 ± 0.8	1.6 ± 0.4*

Values shown are mean ± S.E.M. Single channels records analyzed and displayed as in Supplementary Table 2.
Total events (# of patches): **N1/N2A**, 3,734,783 (14); N1(N616S)/N2A, 553,113 (4); N1(N616A)/N2A 659,173 (5); N1/N2A(N614S) 846,589 (4); N1/N2A(N614A) 868,249 (5).

Tagged values are significantly less (or faster) *(*$p < 0.05$, **$p < 0.01$, or ***$p < 0.001$)* or greater (or slower) *(^$p < 0.05$, ^^$p < 0.01$, or $p < 0.001$)* than wild type (*t-test*) *two-tailed Student's t-test, unpaired*).

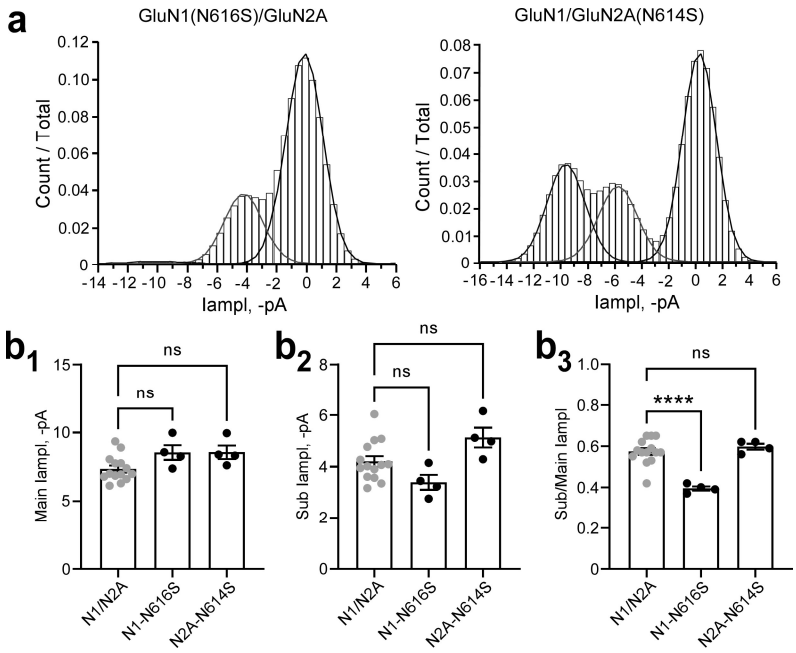

Supplementary Figure 5 (relates to Figure 7). Current amplitudes for main and subconductance levels for wild-type and disease-associated variants (N-to-S) at the GluN1 and GluN2A N-sites.

(a) Amplitude histograms for GluN1/GluN2A (*left*) and GluN1(M641I)/GluN2A (*right*). Fits highlight the closed and main conductance levels (black lines) or the subconductance level (red line).

(b) Bar graphs (mean ± SEM) showing current amplitudes for main (**b**$_1$) and subconductance (**b**$_2$) and the ratio between the Sub and Main (Sub/Main) conductance levels (**b**$_3$) for GluN1 M641 variants co-expressed with GluN2A.

Statistical comparisons were performed using one-way ANOVA with post hoc Dunnett tests versus wild-type (**p < 0.01, ***p < 0.005, ****p < 0.001, ns not significant).

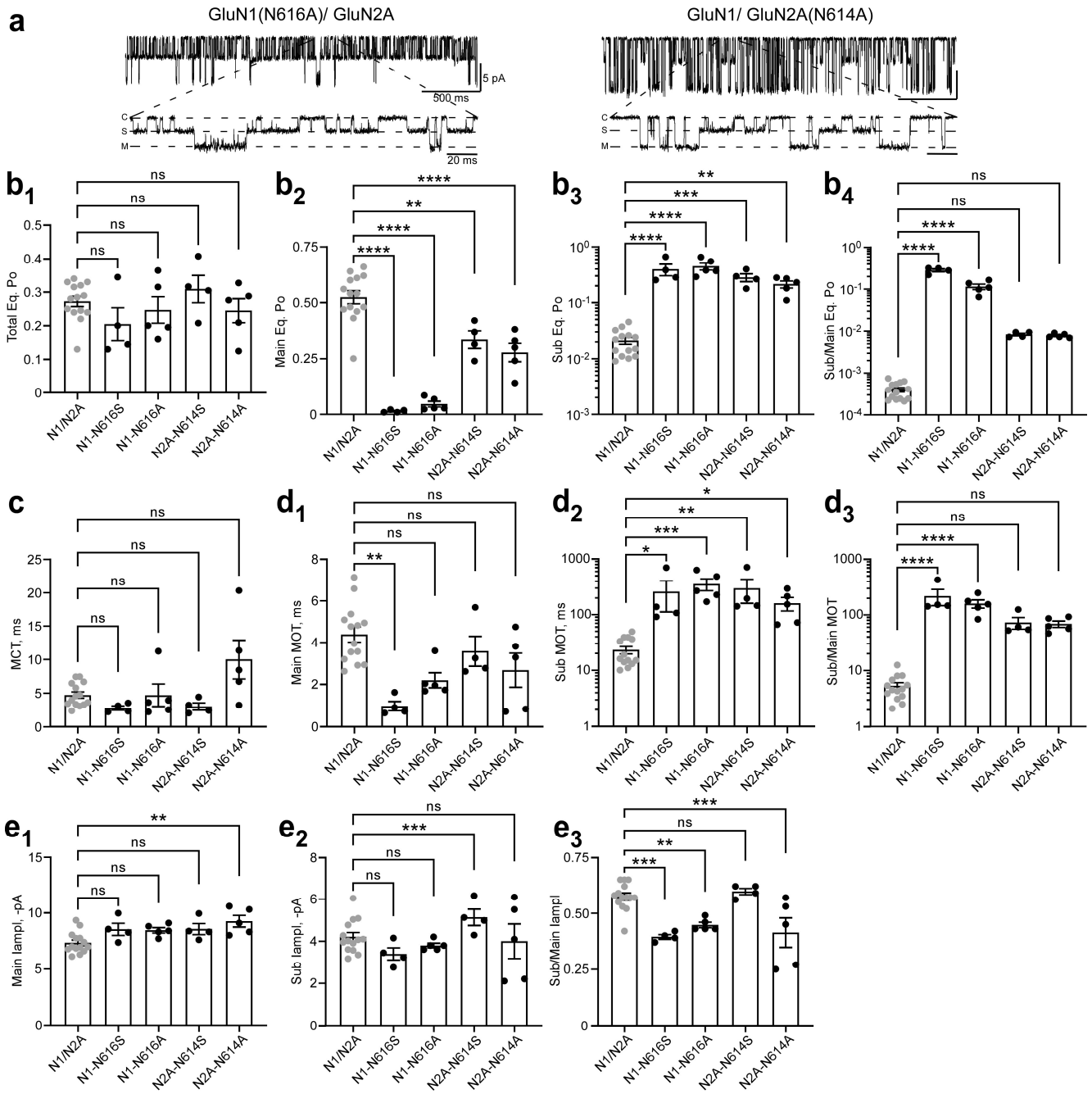

Supplementary Figure 6 (relates to Figures 7 and 8). Mutations (N-to-A) at the GluN1 and GluN2A N-sites induce subconductance states.

(a) Single-channel currents from N-to-A mutations, which are not disease-associated variants, GluN1(N616A)/GluN2A and GluN1/GluN2A(N614A). Data recorded and displayed as in Figure 3a.

(b) Bar graphs (mean ± SEM) showing equilibrium open probabilities for constructs in panel a.

(c & d) Bar graphs (mean ± SEM) showing MCT (**c**) and MOT (**d**).

(e) Bar graphs (mean ± SEM) showing single channel current amplitudes (I_{ampl}) for main (**e1**) and subconductance (**e2**) levels and the ratio of the sub-to-main (**e3**).

For comparison, we include the variants (N-to-S) (Figure 7) and mutations (N-to-A) at the GluN1 and GluN2A N-sites in all bar graphs.

Statistical analysis was performed as in Figure 3. Statistical comparisons were performed using one-way ANOVA with post hoc Dunnett tests versus wild-type (*$p < 0.05$, **$p < 0.01$, ***$p < 0.005$, ****$p < 0.001$, ns not significant).

Supplementary Table 6 (relates to Figure 8f-h). Single channel cluster analysis of wild-type GluN1/GluN2A, GluN1(M641I)/GluN2A, and GluN1(M641L)/GluN2A.

Construct (# of patches analyzed)	T_{crit} *ms*	Cl. P_{open}	MCT *ms*	Cluster length *s*	Intercluster length *s*	$P_{cluster}$
N1/N2A (17)	72 ± 6	0.73 ± 0.02	1.7 ± 0.1	8.8 ± 1.3	2.5 ± 0.2	0.75 ± 0.02
N1(M641I) (15)	585 ± 97^^^	0.61 ± 0.04*	8.1 ± 1.3^	7.5 ± 2.5	2.5 ± 0.3	0.67 ± 0.03
N2A(M641L) (7)	305 ± 89^	0.73 ± 0.03	1.7 ± 0.1	9.9 ± 2.8	2.4 ± 0.5	0.76 ± 0.06

Data set encompasses Supplementary Table 1 but also additional N1/N2A and N1(M641I)/N2A recordings for other aspects of the project. Single channel records were analyzed using T_{Crit} (see Materials & Methods) to identify clusters. Values shown are mean ± SEM for T_{crit}, cluster open probability (Cl. P_o), mean closed time (MCT cluster length, intercluster length, and $P_{cluster}$.

Tagged values are significantly less (or faster) *(*$p < 0.05$)* or greater (or slower) *(^$p < 0.05$, or ^^^$p < 0.001$)* than wild type (*t-test*) *two-tailed Student's t-test, unpaired*)

References for Supplemental Material

Colquhoun D & Hawkes AG. (1990). Stochastic properties of ion channel openings and bursts in a membrane patch that contains two channels: evidence concerning the number of channels present when a record containing only single openings is observed. *Proc R Soc Lond B Biol Sci* **240,** 453-477.

Dravid SM, Prakash A & Traynelis SF. (2008). Activation of recombinant NR1/NR2C NMDA receptors. *J Physiol* **586,** 4425-4439.

Farwell KD, Shahmirzadi L, El-Khechen D, Powis Z, Chao EC, Tippin Davis B, Baxter RM, Zeng W, Mroske C, Parra MC, et al. (2015). Enhanced utility of family-centered diagnostic exome sequencing with inheritance model-based analysis: results from 500 unselected families with undiagnosed genetic conditions. *Genet Med* **17,** 578-586.

Li D, Yuan H, Ortiz-Gonzalez XR, Marsh ED, Tian L, McCormick EM, Kosobucki GJ, Chen W, Schulien AJ, Chiavacci R, et al. (2016). GRIN2D Recurrent De Novo Dominant Mutation Causes a Severe Epileptic Encephalopathy Treatable with NMDA Receptor Channel Blockers. *American journal of human genetics* **99,** 802-816.

Nebet ER, Aprea C, Zoodsma JD, Raab WJ, Sirotkin HI & Wollmuth LP. (2025). Conservation of human NMDA receptor subunits and disease variants in zebrafish. *BMC Genomics* **26,** 1042.

Ohba C, Shiina M, Tohyama J, Haginoya K, Lerman-Sagie T, Okamoto N, Blumkin L, Lev D, Mukaida S, Nozaki F, et al. (2015). GRIN1 mutations cause encephalopathy with infantile-onset epilepsy, and hyperkinetic and stereotyped movement disorders. *Epilepsia* **56,** 841-848.

Pironti E, Granata F, Cucinotta F, Gagliano A, Efthymiou S, Houlden H, Salpietro V & Di Rosa G. (2018). Electroclinical history of a five-year-old girl with GRIN1-related early-onset epileptic encephalopathy: a video-case study. *Epileptic Disord* **20,** 423-427.

Strehlow V, Heyne HO, Vlaskamp DRM, Marwick KFM, Rudolf G, de Bellescize J, Biskup S, Brilstra EH, Brouwer OF, Callenbach PMC, et al. (2019). GRIN2A-related disorders: genotype and functional consequence predict phenotype. *Brain* **142,** 80-92.

Traynelis SF, Wollmuth LP, McBain CJ, Menniti FS, Vance KM, Ogden KK, Hansen KB, Yuan H, Myers SJ & Dingledine R. (2010). Glutamate receptor ion channels: structure, regulation, and function. *Pharmacol Rev* **62,** 405-496.

von Stulpnagel C, Ensslen M, Moller RS, Pal DK, Masnada S, Veggiotti P, Piazza E, Dreesmann M, Hartlieb T, Herberhold T, et al. (2017). Epilepsy in patients with GRIN2A alterations: Genetics, neurodevelopment, epileptic phenotype and response to anticonvulsive drugs. *Eur J Paediatr Neurol* **21,** 530-541.

XiangWei W, Kannan V, Xu Y, Kosobucki GJ, Schulien AJ, Kusumoto H, Moufawad El Achkar C, Bhattacharya S, Lesca G, Nguyen S, et al. (2019). Heterogeneous clinical and functional features of GRIN2D-related developmental and epileptic encephalopathy. *Brain* **142,** 3009-3027.

Xu Y, Song R, Chen W, Strong K, Shrey D, Gedela S, Traynelis SF, Zhang G & Yuan H. (2021). Recurrent seizure-related GRIN1 variant: Molecular mechanism and targeted therapy. *Annals of clinical and translational neurology* **8,** 1480-1494.

Xu Y, Song R, Perszyk RE, Chen W, Kim S, Park KL, Allen JP, Nocilla KA, Zhang J, XiangWei W, et al. (2024). De novo GRIN variants in M3 helix associated with neurological disorders control channel gating of NMDA receptor. *Cellular and molecular life sciences : CMLS* **81,** 153.